ELSEVIER

Journal of Electroanalytical Chemistry 380 (1995) 91–107

JOURNAL OF ELECTROANALYTICAL CHEMISTRY

Calorimetric and nuclear byproduct measurements in electrochemical confinement of deuterium in palladium

D. Gozzi *[,a], R. Caputo [a], P. Luigi Cignini [a,1], M. Tomellini [a,2], G. Gigli [a], G. Balducci [a], E. Cisbani [b], S. Frullani [b], F. Garibaldi [b], M. Jodice [b,3], G. Maria Urciuoli [b,3]

[a] *Dipartimento di Chimica, Università La Sapienza, Ple Aldo Moro 5, 00185 Roma, Italy*
[b] *Laboratorio di Fisica, Istituto Superiore di Sanità, Vle Regina Margherita 299, 00161 Roma, Italy*

Received 17 February 1994; in revised form 3 June 1994

Abstract

We present the results of a new experiment with our multicell set-up implemented with mass spectrometric measurements of ^{4}He and a highly improved neutron detector. The excess heat measured is comparable with the results of other laboratories, but no neutrons were found and the tritium excess was lower than expected from the power excess. ^{4}He has been measured in the electrolysis gases and a tentative correlation of ^{4}He with excess power is presented and discussed.

Keywords: Cold fusion; Calorimetry; Nuclear byproducts; Deuterium; Palladium

1. Introduction

Since 1989, continuous efforts have been made in various countries around the world to investigate the nature of the excess heat found in electrochemical experiments involving loading palladium or palladium alloys with deuterium. The results of such experiments carried out by several groups over a period of 5 years using different techniques and procedures indicate that the heat power excess findings, up to 3.7 kW cm^{-3} of Pd [1], cannot be attributed to artefacts and their magnitude appears to be well beyond the power that any chemical process could be expected to release. If suitable protocols are used, heat generation is found and quite definite progress has been made towards its reproducibility although adequate control of its onset, duration and magnitude is still difficult. Because these features are the primary conditions for developing any type of technologically exploitable energy-producing device, efforts to improve them are in progress, particularly by private companies, mostly in Japan.

With respect to the recovery of nuclear ash, the overall picture is more intriguing. It has been confirmed that the rates of generation of neutrons and tritium nuclei from the d, d reaction channels, which is believed to be occurring in plasma physics, are several orders of magnitude lower than the values expected from heat power excesses measured by calorimetry. Therefore, in condensed matter, other nuclear byproducts of the d, d reaction must be invoked and sought. Only one other channel, the ^{4}He channel, can exist in this two-body reaction. Since the earliest investigations, various measurements [2–8] to detect ^{4}He both in Pd cathodes and in the gas phase escaping from the electrochemical cells have been reported but only a few of them have been discussed in detail. Up to now only one electrochemical cell experiment has been reported [3] where evidence is given of heat excess roughly correlated with ^{4}He measured in the gas phase. The air contamination which could have occurred in this experiment was discussed in a later publication [5]. Gas loading experiments in a high vacuum assembly have clearly shown the release of ^{4}He when deuterium is confined in Pd between blocking interfaces [6].

From the theoretical point of view, there are at least two major problems to solve in order to explain these

* To whom any correspondence should be addressed.
[1] CNR-Centro di Termodinamica Chimica alle Alte Temperature, c/o Dipartimento di Chimica, Università La Sapienza, Italy.
[2] Dipartimento di Scienze e Tecnologie Chimiche, Università Tor Vergata, Via della Ricerca Scientifica, 00133 Roma, Italy.
[3] National Institute for Nuclear Physics (INFN) sez.Sanità, V.le Regina Margherita 299, 00161 Roma, Italy.

SSDI 0022-0728(94)03607-5

experimental observations: (i) the Coulomb barrier to the d,d reaction between low energy nuclei; (ii) the energy release to the Pd lattice of the α-particle produced. In terms of plasma physics, there is no solution for either of these problems. However, some theories with promising results have been developed [9–12]. Their main feature is the attempt to replace the schemes of the high energy physics which are believed to be inappropriate for the treatment of different physical situations such as that of condensed matter.

The preceding summarizes the data emerging from four international conferences [13–16], several specialized international meetings [17–18] and hundreds of journal publications.

Starting in 1989, our group, which includes expertise on physical chemistry and nuclear physics, has continually been involved in performing multicell experiments providing calorimetric and nuclear (neutrons, tritium, ^{4}He, gammas) measurements as well as some materials science applications to the preparation of Pd cathodes [19–24]. In the present paper we report some of the results [16] obtained in the last multicell experiment which included the quantitative measurement of ^{4}He.

2. Experimental

2.1. Overview

In designing an experiment in such a controversial area one should ideally be able to measure simultaneously and as functions of time all the physical and chemical quantities by independent experimental techniques in order to have complete control of the phenomena occurring in the system under examination. In electrochemical experiments involving loading Pd or Pd alloys with deuterium, it is obvious that the excess power is the key parameter. However, various different reactions have been invoked on the nuclear side and therefore several nuclear signatures are of interest. The d,d plasma fusion reactions have been taken into consideration since the earliest investigations, but neutrons and tritium have been found to be several orders of magnitude lower than the power excess [25,27]. The expected tritium-to-neutron ratio of about unity has never been found; we have reported a value of 10^5–10^6 [20,24], in agreement with the literature [25]. Since 23.8 MeV γ emission which is the signature of the d (d,^{4}He)γ channel, has never been found [20,25,27], a direct release of energy to the lattice was hypothesized. Two experiments (one in electrochemical cells [3]) so far have reported the detection of ^{4}He above the background in the gas phase. ^{4}He has also been found in two cases [7,8] among the very limited number of experiments where electrodes have been analysed. Therefore, taking into consideration the practical difficulties involved in measuring both neutrons and γ radiation simultaneously and with comparable accuracy in our present apparatus, we decided to measure tritium and ^{4}He in the gas phase as well as the power excess and neutrons.

Our experimental is based on a multicell system consisting of up to 10 cells which are identical apart from the cathode material, geometry or preparation. One or more cells can be blanks with the cathode made of a material such as Pt or Au which does not absorb D (H) or made of Pd but immersed in a D-free electrolyte. The cells are connected in series and the electrolysis is carried out in galvanostatic mode (each cell can be excluded from or inserted in the electrical series circuit at any time by a home-made device controlled manually or by computer). Thus the rate of all electrochemical processes is the same in each cell. This procedure results in a number of important conditions related to the calorimetry; for example, the flow rate of the electrolysis products D_2 (g) and O_2 (g) is, according to Faraday's law, equal in each cell [1] so that the heat transported by the escaping gases and the heat necessary to saturate the gases themselves by D_2O (H_2O) are also the same in each cell, provided that the temperature of the solution is the same.

As each cell is a non-adiabatic calorimeter, it is important that the way in which the heat is exchanged with the surroundings is the same for all the cells. As expected, this occurs mostly through the conductive path localized in the glass wall of the cell between the electrolyte solution and the thermostated stream of circulating water. This condition is obtained by positioning all the cells symmetrically in a torus-shaped bath filled with circulating water kept at constant temperature (generally 21.0 ± 0.1°C) by a high quality thermostat.

The torus (50 cm outer diameter and 30 cm inner diameter) is contained in a large neutron counter designed by us and manufactured by Jomar-Canberra, Los Alamos (see below).

A complete flowchart, reported elsewhere [24], allows easy understanding of what is being monitored, what is done in each cell set-up and how the signals are processed. All the cells are treated according to the flowchart. Open-type cells with external recombination are used. The external recombinator coupled to the D_2 (H_2) trap is an efficient D_2 (H_2) removal system (see below).

^{4}He measurement by a magnetic type mass spectrometer [28] is not made on-line and the gas line is sampled discontinuously by filling a 500 ml stainless

[1] Strictly speaking, this is only true when the rate of D (H) absorption by the cathode is zero. For practical purposes, however, this condition is fulfilled quite soon after starting the electrolysis.

steel cylinder. As will be shown later, the gas composition at the sampling stage is given by N_2 with D_2 (H_2), O_2 and D_2O (H_2O) traces and ^4He (if any).

In the following we describe the various parts of the experimental set-up, except for the ^4He measurement procedure which has been reported elsewhere [28], and the procedures adopted, making reference to previous reports [24–26] and discussing in detail the new features and the reliability of the various methods adopted.

2.2. Electrochemical cells and calorimetry

Electrochemical cell

The most recent version of the electrochemical cell was modified with respect to the previous version [26] to make it impervious to air contamination in view of ^4He measurements. To carry ^4He up to the sampling cylinder, owing to the deuterium removal system (see later), we have to use a N_2 stream from a liquid N_2 tank. This ensures a low ^4He background [28].

The cell geometry (inner diameter 22 mm and height 245 mm) was designed to maximize the heat transfer in the radial direction. The effective volume of the cell to be filled with the electrolyte solution was about 53 ml. Small deviations from this value may exist from cell to cell if the cathodes differ in size.

Two K-type thermocouples were placed in the cell to measure the temperature of the cathode and the solution, and one was placed just outside the cell in a massive copper ring immersed in the thermostated bath. Automatic computer-controlled refilling of D_2O (H_2O) is operated by the liquid sensor level positioned in the lateral tube.

To ensure good permanent coaxial positioning of the electrodes, both the cathode and anode were partially inserted in an appropriately machined Teflon piece which also acted as a N_2 scrubber.

The anode was a coil of inner diameter 12 mm and height comparable to that of the cathode made from 1 mm diameter Pt wire.

The electrolyte solution was 0.2 M LiOD in 99.99% D_2O (ISOTEC, USA) at low tritium content (ca. 1 Bq ml^{-1} or 60 dpm ml^{-1}). Inductively coupled plasma atomic emission spectroscopy (ICPAES) analysis of the starting solution did not reveal any alkaline or heavy metal above the detection limit, which is generally 10 ppb or less.

Some of the features of the cells used in this experiment are given in Table 1. All the Pd cathodes were machined from rods supplied by Johnson and Matthey (UK).

Calorimetry

The calorimetric excess heat measurements were based on a comparison of the actual value of temperature of the solution at a given input power with the calibration curve. The calibration curve was obtained by increasing or decreasing the input power stepwise. This can be done either in thermal mode, using the inner heater, or in electrochemical mode, using Au or Pt cathodes under exactly the same conditions as those under which the experiment is subsequently carried out. A detailed discussion of these procedures has been previously reported [25,26], and therefore we limit ourselves to giving the coefficients of the calibration equations for the cells used in this experiment in Table 2. All the relations are straight lines with a high correlation factor r, and have the general form

$$P_{in} = (a_i \pm \Delta a_i) + (b_i \pm \Delta b_i)\Delta T_i$$

where

$$\Delta T_i = \left(T_s - T_s^0\right)_i - \left(T_{tb} - T_{tb}^0\right)_i$$

and T_s and T_{tb} are respectively the temperatures of the solution and of the thermostated bath just outside the cell and measured in the copper ring, T_s^0 and T_{tb}^0 are the respective values of T_s and T_{tb} at $P_{in} = 0$, P_{in} is the input power which is equal to IV_{in} or $I(V_{in} - V_{th})$ depending on whether the cell is powered in the thermal or the electrochemical mode, $V_{th} = \Delta H^\circ/2F$ is the

Table 1
Some features of the cells tested in this experiment

Cell no.	Cathode material and size (∅ × h)/mm	Treatment	Gas line material	Comment
1	Pt 1 × 23	As received	Stainless steel	Blank
2	Pd 2 × 25	As received	Nylon	
4	Au + Pd 6 × 23	High vacuum at mp of Au	Stainless steel	D_2 confinement experiment [32]
7	Pd 2 × 21	Screw dislocated	Nylon	Switched on from 675 to 930 h
8	Pd 3 × 22	Screw dislocated	Nylon	
10	Pd 3 × 23	As received	Nylon	

Table 2
Coefficients of the calibration curves $P_{in} = (a_i \pm \Delta a_i) + (b_i \pm \Delta b_i)\Delta T_i$

Cell no. i	a_i/W	Δa_i/W	b_i/W K^{-1}	Δb_i/W K^{-1}	r	$P_{exc,i}^{min}$/W
1	0.7	0.5	7.0	0.1	0.9983	1.7 ± 0.7
2	0.3	0.7	5.8	0.1	0.9985	1.2 ± 0.8
4	0.06	0.60	5.5	0.1	0.9979	0.9 ± 0.7
7	0.5	0.3	5.06	0.07	0.9993	1.3 ± 0.3
8	−0.6	0.4	5.21	0.09	0.9991	0.2 ± 0.4
10	−0.5	0.9	6.3	0.2	0.9968	0.4 ± 0.9

All the coefficients given are the average of the values obtained by the thermal and electrochemical calibrations.

thermoneutral potential, $\Delta H°$ is the enthalpy of decomposition of D_2O (H_2O) and F is the Faraday constant. The value of V_{th} adopted is 1.5367 V [29]. V_{in} and I are respectively the electrical potential difference at the leads read closest to the heating resistor, in the thermal mode, or at the electrodes, in the electrochemical mode, and the current measured as the voltage drop at the leads of a high precision 100 mΩ resistor. The overall uncertainty in measuring P_{in} is 0.01%. The reproducible linear behaviour of the calibration curves over a wide range of input power values strongly supports the assumption that the actual path of heat transfer is very close to that expected.

The heat power excess P_{exc} of cell i is given by

$$P_{exc,i} = P_{out} - P_{in} = a_i + b_i\Delta T_i - P_{in} \quad (1)$$

where ΔT_i is now the value measured in the experiment. The overall error in P_{exc} has been evaluated to be less than ±10% [25]. The minimum heat power excess detectable is given by

$$P_{exc,i}^{min} \geq (a_i \pm \Delta a_i) + (b_i \pm \Delta b_i)\Delta(\Delta T_i)$$

where $0.1°C < \Delta(\Delta T_i) \leq 0.2°C$, is the minimum temperature change detectable by the K-type thermocouples used. The $P_{exc,i}^{min}$ values in Table 2 were calculated assuming that $\Delta(\Delta T_i) = 0.15°C$. Note that, owing to the definition of ΔT_i, the systematic error in this quantity is practically zero.

The energy balance of the calorimeter during a calibration input power step is given by

$$P_{in} = m_s C_s \frac{\partial \Delta T_i}{\partial t} + \frac{\pi dk_{Pyrex}}{l} h\Delta T_i(t) + \frac{k_{rad}}{\pi dh}\left\{[T_{tb} + \Delta T_i(t)]^4 - T_{tb}^4\right\} + \left(\frac{3I}{4F} + \frac{P}{RT_r} f_{N_2}\right)\left[\frac{p(t)}{P - p(t)}\right] \times \left[(C_g - C_l)_{D_2O}\Delta T_i(t) + \Lambda_{D_2O}\right] \quad (2)$$

where the four terms on the right-hand side represent the rate of enthalpy change of the solution, the rate of heat transfer from the solution to the thermostated bath by conduction through the Pyrex wall, the rate of heat transfer by radiation to the thermostated bath and the rate of heat transfer from the solution to the gases (produced by electrolysis + N_2 carrier) escaping from the cell and saturated with D_2O (H_2O) at the temperature of the solution (the symbols in Eq. (2) are defined in Appendix A). Owing to the continuous heat transfer to the thermostated bath, ΔT_i is generally below 15°C, in contrast with its value in an adiabatic calorimeter [1], and therefore the vapor pressure of D_2O (H_2O) is low with respect to the atmospheric pressure and the term $p(t)/[P - p(t)] = 2 \times 10^{-2}$. The sign of the last contribution to the sum of the right-hand side of Eq. (2) depends on the sign of the term $[(C_g - C_l)_{D_2O}\Delta T_i(t) + \Lambda_{D_2O}]$ which is always positive in the useful working temperature range (it becomes negative at $\Delta T_i(t) = -\Lambda_{D_2O}/[(C_g - C_l)_{D_2O}] > 906.5°C$), whereas the overall magnitude can be evaluated as close to ca. 4.5 mW for $I < 1$ A and $f_{N_2} = 5.4 \times 10^{-7}$ m^3 s^{-1} at stp (see below).

The radiative term $(k_{rad}/\pi dh)\{[T_{tb} + \Delta T_i(t)]^4 - T_{tb}^4\}$, for the same conditions on ΔT_i as given above, is evaluated as ranging around 3 mW, and therefore for practical purposes Eq. (2) can be written as

$$P_{in} \approx m_s C_s \frac{\partial \Delta T_i}{\partial t} + \frac{\pi dk_{Pyrex}}{l} h\Delta T_i(t) \quad (3)$$

It is important to point out that, in the determination of P_{exc}, the energy balance could be expressed in the form

$$P_{exc,i} = m_s C_s \frac{\partial \Delta T_i}{\partial t} + \frac{\pi dk_{Pyrex}}{l} h\Delta T_i(t) + \Phi[\Delta T_i(t)] - P_{in,i}(t) \quad (4)$$

where are now included the sum of both the terms previously neglected in the term $\Phi[\Delta T_i(t)]$. It is easy to verify that the elimination of $\Phi[\Delta T_i(t)] > 0$ from Eq. (4) always produces an underestimation of P_{exc}.

The integration of Eq. (3), in the case of a calibration step of input power, gives

$$\Delta T_i = \frac{\tau P_{in}}{\zeta}\left[1 - \exp\left(-\frac{t}{\tau}\right)\right] = \Delta T_{i,(t\to\infty)}\left[1 - \exp\left(-\frac{t}{\tau}\right)\right]$$

$$\tau = \left(\frac{\pi dhk_{Pyrex}}{l\zeta}\right)^{-1} \qquad \zeta = m_s C_s \quad (5)$$

$$\Delta T_{i,(t\to\infty)} = \left(\frac{\pi dhk_{Pyrex}}{l}\right)^{-1} P_{in}$$

where the term $(\pi dhk_{\text{Pyrex}}/l)^{-1}$ is the slope of the calibration curve which corresponds to the $(b_i)^{-1}$ parameters shown in Table 2. The expected time constant value is $\tau = \zeta/b_i = \rho_l V^0 C_l/b_i M \approx 280/b_i$ s. Higher values (350–400 s) of τ are found experimentally because the ζ term should be written more correctly as $\zeta = m_s C_s + \Sigma m_k C_k$ where the summation includes all the masses present in the cell. A set of points obtained under stationary conditions of ΔT_i associated each time with a different P_{in} value, provided that h is kept constant by a level sensor, must lie, within experimental error, on a straight line of slope $(\pi dhk_{\text{Pyrex}}/l)^{-1}$ since this value depends only on constant quantities. This is just what we obtained, as shown in Table 2. The validity of the treatment above can be checked by obtaining k_{Pyrex} from the slope of the calibration curve. The average value obtained is 0.9 ± 0.1 W m^{-1} K^{-1}, which is in agreement with the value reported in literature [30] (see Appendix B).

2.3. Deuterium removal system

The deuterium removal system consists of a catalytic recombinator and a Pd sponge trap connected in series by stainless steel tubing (inside diameter, 1.5 mm) or nylon 66 tubing (inner diameter, 3 mm). This system allows us to measure tritium in the electrolysis gas (see below) and to reduce D_2 in the gas stream before sampling for ^{4}He analysis.

Catalytic recombinators

The catalytic recombinators are described elsewhere [25]. Their yield η is calculated from the equation

$$\eta = \frac{v_{\text{rec}}}{v_{\text{cons}}} = \frac{v_{\text{meas}} - f_{\text{cond}}\Delta t}{(\bar{v}/2F)\int_{\Delta t} I\,\mathrm{d}t} \tag{6}$$

measuring the recombined volume of D_2O in the time interval Δt. The correction for the condensation of D_2O contained in the gas stream was measured to be 3.75×10^{-6} cm^3 s^{-1}. The recombination yield value averaged over 10 recombinators is about 92%.

The partial pressure values of D_2 at the recombinator inlet and outlet are derived from the equations

$$P_{D2}^{\text{in}} = \frac{I/2F}{(P/RT_r)f_{N_2} + (3I/4F)}P$$
$$P_{D_2}^{\text{out}} = \frac{(I/2F)(1-\eta)}{(P/RT_r)f_{N_2} + (3I/4F)(1-\eta)}P \tag{7}$$

Assuming $I = 1$ A, $\eta \approx 0.9$ and using the data in Appendix B, we obtain $P_{D_2}^{\text{in}}$ and $P_{D_2}^{\text{out}}$ values of 1.74×10^{-1} P and 2.28×10^{-2} P respectively. The latter value is the D_2 partial pressure of the gas stream entering the Pd sponge trap.

Pd sponge trap

Two equal traps, working alternately and continuously fluxed under a N_2 carrier during regeneration, are made of a stainless steel cylinder with an inner coaxial stainless steel tube. The path of the gas mixture inside the trap is such that the largest contact surface area with the Pd sponge is ensured. Each trap contains about 150 g of Pd sponge (Johnson-Mattey, UK).

If we assume that the absorption reaction

$$\mathrm{Pd(s)} + \frac{y}{2}\mathrm{D_2(g)} = \mathrm{PdD}_y\mathrm{(s)} \tag{8}$$

is completely shifted to the right-hand side, we can define the nominal capacity of the trap as $C_{\text{trap}} = yw_{\text{Pd}}/2M_{\text{Pd}}$. Therefore, the residual capacity of the trap with respect to the initial capacity, as a function of D_2O consumed, is given by

$$C_r = 1 - \frac{1-\eta}{\bar{v}C_{\text{trap}}}v_{\text{cons}} \tag{9}$$

It is easy to see that electrolysis of just 8.5 cm^3 of D_2O would be sufficient to exhaust a Pd trap in the case of $\eta = 0$. However, in our case $\eta \approx 0.90$, and hence electrolysis of 10 times more D_2O would be necessary to exhaust the trap completely.

The minimum partial pressure of D_2 in the gas stream at the outlet of the Pd trap should be equal to the activity of D_2(g) in the gas phase in thermodynamic equilibrium with the condensed phase at a certain activity of D according to reaction (8). This value can be calculated from the following equation [31]:

$$\ln a_{D_2} = \left[-\frac{\Delta H_{\text{abs}}(y)}{RT_r}\right] + 2\ln\left(\frac{y}{1-y}\right) + \frac{\Delta S^0_{\text{abs}}}{R} \tag{10}$$

As reported elsewhere [32], the background pressure of D_2 at the outlet of the Pd trap, measured by mass spectrometry, has been found to be ca. 5×10^{-10} atm which, by Eq. (10), corresponds to $y \approx 0.2$. Therefore the overall removal factor of D_2, present in the N_2 carrier at the outlet of the electrolysis cell, is about 10^8. This remarkable result, combined with the high resolution power of mass spectrometry, allows us to be very confident about the quantitative determinations of both ^{4}He and D_2.

2.4. Measurements of nuclear byproducts

Tritium

To prevent any air contamination, in contrast with previous experiments, we did not perform tritium tests in the electrolytic solutions of the cells but only in the D_2O produced by the catalytic recombinators. The experimental procedure adopted to measure tritium

and the calculation used to evaluate the tritium electrolytic enrichment in the solution have been described elsewhere [24]. Because in this experiment the tritium measurement is performed on the recombined gases and a carrier gas is present in addition to the electrolysis gases, correct evaluation of the effects of the electrolysis on the tritium concentration in the gas stream requires a modification of the mathematical treatment utilized in the past.

Considerations based on the mass balance of tritium in our cells lead to the following differential equation:

$$\frac{dx}{dt} = n_{D_2O}\left[x_f f_{D_2O} - \frac{I}{2F\alpha_E}x - \frac{p}{\alpha_V(P-p)}f_G x - x\frac{dn_{D_2O}}{dt}\right] \quad (11)$$

As stated in the preceding section, the volume of the electrolyte must be constant; therefore the term $dn_{D_2O}/dt = 0$, and consequently the D_2O feed, must compensate the D_2O consumed by the electrolysis and the D_2O evaporated in the gas stream escaping from the cell. If, as normally occurs, the molar fraction of DTO in the D_2O feed is the same as that in the D_2O initially present in the electrolytic solution, integration of Eq. (11) gives

$$q = q_{lim} - \left(q_{lim} - \frac{1}{\alpha_E}\right)\exp\left[-\frac{v_{cons}(I,t)}{V^*}\right] \quad (12)$$

where the quantity $q = x_g/x^0$ represents the expected change, due only to the electrolysis, of the atomic fraction of tritium in the gas phase with respect to the initial atomic fraction of tritium in the electrolyte. In Eq. (12) the terms q_{lim} and V^* are given by the following expressions:

$$q_{lim} = \frac{1 + (3/2 + 2FPf_{N_2}/RT_rI)[p/(P-p)]}{1 + (\alpha_E/\alpha_V)(3/2 + 2FPf_{N_2}/RT_rI)[p/(P-p)]} \quad (13)$$

$$V^* = \frac{\alpha_E V^0}{1 + (\alpha_E/\alpha_V)(3/2 + 2FPf_{N_2}/RT_rI)[p/(P-p)]} \quad (14)$$

At fixed temperature and carrier gas flow rate, an important difference between Eq. (12) and Eq. (2) of ref. [24] (obtained for tritium enrichment in the electrolyte) is that q_{lim} and V^* are also functions of the electrolysis current, whereas the corresponding terms α and β are constants. By inspection of Eqs. (12)–(14), the following remarks can be made:

at $v_{cons} \to 0$,

$$q = 1/\alpha_E \quad (15a)$$

at $v_{cons} \to \infty$,

$$q = q_{lim} \Rightarrow \begin{cases} f_{N_2} = 0 \Rightarrow \dfrac{1}{\alpha_E}\left\{\dfrac{1 + (3/2)[p/(P-p)]}{1/\alpha_E + (3/2\alpha_V)[p/(P-p)]}\right\} \\ \quad \approx \dfrac{1}{\alpha_E}\alpha_E \approx 1 \\ I = 0 \Rightarrow \dfrac{\alpha_V}{\alpha_E} \approx \dfrac{1}{\alpha_E} \end{cases} \quad (15b)$$

Therefore the expected q vs. v_{cons} curve starts from $1/\alpha_E$ and remains at this value if $I = 0$ or tends to unity in the case of electrolysis without any carrier gas stream, whatever the value of I. Since α_E depends mostly on the nature of cathode ($\alpha_E = 1.8$ on Pd [24,25]), it is expected that the limits for q will be in the range from ca. $1/2$ to 1. In this experiment, $f_{N_2} \neq 0$ and is kept constant, whereas I was changed and in some cases switched off for a certain period of time, as will be shown in the results section. Therefore we have to expect that, throughout the experiment, if tritium is not generated in the cell by a nuclear reaction, the value of q must be within the range $1/\alpha_E \leq q < 1$. Further aspects will be discussed in Section 4.

Helium-4

The reliability of the ^{4}He measurements is discussed in a separate publication [28]. It is sufficient to report here that, from the point of view of the ^{4}He measurement alone, cells 2, 7 and 8 did not exhibit sufficiently prominent features to be considered significant. However, ^{4}He concentrations definitely greater than the background have been detected in the gases escaping from cells 4 and 10. ^{4}He concentrations at the background level were observed for the reference cell 1 all through the experiment. The controls which have been made with the simultaneous measurements of ^{20}Ne favoured the occurrence of air contamination as the simplest explanation, but in this respect the overall experimental picture did not satisfactorily agree with such a conclusion [28].

Neutrons

A description of our more recent system for neutron detection has already been given [24]. The neutron detector was designed and manufactured, according to our specifications, by Jomar Systems Division of Canberra Industries Inc. It consists of 60 ^{3}He-proportional tubes of active length 41 cm, diameter 2.54 cm and gas pressure 6 atm. These tubes are embedded in a cylindrical polyethylene moderator. The detector is segmented in 12 independent counters consisting of five tubes each, arranged in inner and outer rings of six

counters. The positions of the central tubes of each counter are stacked at half-counter length between the inner and outer ring (see Fig. 8 below). The torus containing the 10 electrolytic cells is surrounded by the detector, and the cell from which the neutron emission originates can be identified by analysis of the pattern of counts registered by the 12 different counters. If the emission is burst-like, the time-correlated counts (with time correlation consistent with the decay time of the detector) should affect contiguous numbered counters of the inner and outer rings facing the cell where the emission has occurred. The efficiency of the detector measured with a californium-252 source placed in the different positions of the 10 cells is 18%. The dependence of the efficiency on the cell position is limited to less than 1%. The counts are essentially distributed among three or four contiguous numbered counters shared between the inner and outer rings. This distribution allows identification of the emitting cell if neutron bursts occur or if random generated neutron emissions happen at a rate substantially higher than the background. In the present experimental conditions the background of the whole detector is about 0.8 counts s^{-1}, i.e. about 0.2 counts s^{-1} in a group of four contiguous numbered counters.

The signals from each group of five tubes were processed by an AMPTEK A-111 hybrid charge-sensitive pre-amplifier–discriminator which gives, as the output of the counter, both the digital and the linear OR of the five tubes. The digital output of each counter is sent to two scalers, of which one is read and reset at a fixed time interval, and the other is read and reset only at the end of a run lasting several days. The output is also sent to a pattern unit in order to detect all the counters fired within the time allowed by the acquisition cycle time (at present of the order of 1 ms). Moreover, it is used to obtain a logical OR of all 12 counters which is sent to the JSR-12 (Jomar Shift Register) neutron coincidence analyser. The main purpose of the JSR-12 is to act as a filter in order to enhance the capability of detecting time-correlated counts through its scaler R. In fact, each time a neutron is detected, a scaler T (total) is incremented by a single count and two intervals of time are opened, the first starting a few microseconds after the detection and the second after about 1 ms. Both random neutrons and neutrons correlated with that neutron that has allowed the gate to be opened are expected in the first gate, while only random neutrons are expected in the second gate owing to the large interval of time which has elapsed with respect to the decay time of the detector. The counts in the first gate increment the R + A (real + accidentals) scaler of the JSR-12 in non-linear way, while those in the second gate increment the A scaler. The two gates are opened for each neutron detected; then the increment of R + A is equal to the sum of the neutrons detected in each opened gate. When N neutrons are emitted in a very short time interval and all are detected within the time interval of a single gate, the increment of the R + A scaler is equal to $N(N-1)/2$. Comparison of the R + A and A scalers allows the number of correlated neutrons to be estimated.

The 12 analogue signals from the 12 counters are amplified and then sent to a linear fan-in fan-out from which two linear ORs of these signals are produced. The first goes to a waveform digitizer, i.e. a digital oscilloscope, which permits acquisition of the information on each pulse including the absolute time (given with a precision of nanoseconds) and the waveform; the second goes to an analogue–digital converter (ADC) that digitizes its integral and sends the value obtained directly to a histogramming memory. Scaler, pattern unit, ADC and histogramming memory are CAMAC modules and are read through a CAMAC bus by a crate controller driven by a Macintosh personal computer through a GPIB IEEE port that also drives the oscilloscope. The computer reads the pattern unit at each occurrence of the CAMAC Look At Me (LAM) signal and reads the histogramming memory and the scalers every 10 min. The LAM signal is emitted when the pattern unit has received at least one logic pulse from the detector.

Data acquisition system

Two separate data acquisition systems are now used in our experiments (only one was used in the past [24]). Both are based on the network Macintosh computer ⇔ IEEE-488 and RS-232 interfaces ⇔ instruments. They are dedicated first to neutron acquisition (see above and ref. [24]) and second to the acquisition and control [24] of all the other devices and sensors in the experimental set-up (mostly through a data logger). The programs running on each of the two systems were home-made, both realized on LabVIEW 2.1.1 software from National Instruments (Austin, TX). All the temperature, voltage, current and other analogue signals go to the analogue input channels of the data logger (Orion 3531 D, Schlumberger, UK) and are logged at fixed scan intervals. Generally the scan interval time is set at 300 s, but it can change automatically to 5 s if an alarm occurs on one of the logged channels. The alarm feature is based on a preset threshold. All the channels connected to the cathode and solution thermocouples of each cell, as well as the counter-channel connected in parallel to the transistor–transistor logic (TTL) OR of the neutron counter, are set to generate alarms. The primary file (the program also generates other ancillary files such as those containing dates and D_2O refilling volumes of each cell) for every item of data acquisition comprises a matrix of 1000 rows × 60 columns which is built by append mode on both the random access

memory (RAM) and removable hard discs. Real time plotting of all the channels is available on the computer screen.

Finally, as already mentioned, since the complete cell system is positioned inside the neutron detector, a monochrome TV camera, connected to a video recorder, is placed in the centre of the torus and operated by both manual and automatic remote control (by data logger) so that the status of each cell is under more direct control.

3. Results

3.1. Calorimetric and ^{4}He data

As mentioned above, and described fully elsewhere [28], because of the detection of ^{20}Ne, the ^{4}He results should be considered with great caution owing to the possible occurrence of at least partial air contamination. Nevertheless, as will be made clear below, we believe that it is useful to report the comparison of these data and the calorimetric results because a very interesting, also if somewhat intriguing, picture emerges from the overall experiment.

All the data presented in the text were obtained using the stepwise electrolysis current patterns shown in Fig. 1 for all the cells tested.

Figs. 2–5 show graphs representing the ^{4}He and calorimetric results throughout the experiment for some cells. Each figure shows from the top to the bottom the input power, heat power excess and ^{4}He concentration, given in parts per billion, compared with the ^{4}He concentration in the blank cell. Heat power excess has been calculated according to Eq. (1) and Table 2, and the related error has to be considered conservatively equal to $\pm 10\%$ of the value while the error on the input power is, as already mentioned, negligible. Because of the large number of points composing each curve ($> 10^4$), for clarity the errors bars are not reported in the middle plots. To facilitate a comparison of the energy quantities involved, the scales of input power and heat power excess plots are the same. Furthermore, the lack of heat excess results in some parts of the related curve is due to a conservative approach that we adopted in rejecting those data which were acquired in experimental conditions not exactly equal to those in which the calibration curve had been obtained [2]. The error in the ^{4}He concentration has been estimated to be $\pm 13\%$ of the value [28]. Cells 1 and 7 did not show any excess heat power within the limits of experimental error. This is as expected for cell

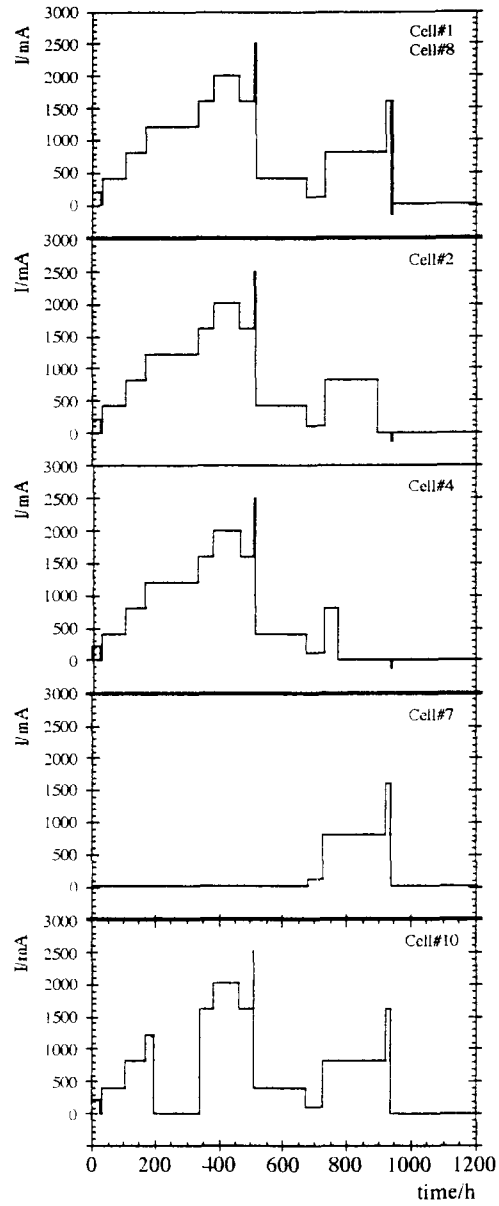

Fig. 1. Time chart of the electrolysis current applied to the cells in Table 1.

1 because it is the blank cell. Cell 7 was switched on in the final part of the experiment (no particular attention was part to the charging protocol) to obtain further information aimed at understanding the effect of a change in gas composition, due to electrolysis, on the mechanism of a possible contamination by air. In this case, the line was continuously flushed with the carrier gas for more than 700 h.

Figs. 2–5 show that the maximum value of heat power excess in each cell was in the range from 2 to 19 W ($\pm 10\%$) and the ratio Γ of excess power to input power ranged from 0.13 to 0.70. These figures and others extracted from the plots above are reported in Table 3.

[2] Related to some electrical perturbations induced during the D_2 confinement experiment on cell 4 [32].

It must be pointed out here that, for the reasons described separately [28], all the ^{4}He data taken after 900 h of the experiment were conservatively discarded.

3.2. Tritium data

Tritium data are reported in Figs. 6 and 7 which show five equivalent graphs, each giving $q^{\#}_{th}$, as calculated by Eq. (12), $q^{\#}_{exp}$ measured in the recombined gases (we recall that $q^{\#}_{exp} = x^{\#}_g / x^0$) and those values of the difference $(q^{\#}_{exp} - q^{\#}_{th})$ satisfying the condition $(q^{\#}_{exp} - q^{\#}_{th}) \geq \Delta x_g / x^0 = 5/80 = 6.25 \times 10^{-2}$, where Δx_g is the experimental error on the measurement, given in dpm ml^{-1}, of the atomic fraction of tritium in the recombined D_2O. In considering the plot of cell 1, it must be remembered that the theoretical equation has been calculated assuming $\alpha_E(Pt) = \alpha_E(Pd)$. Since, notwithstanding the criterion adopted before in discriminating $(q^{\#}_{exp} - q^{\#}_{th})$ values, some $(q^{1}_{exp} - q^{1}_{th})$ values were still found to be greater than zero, the quantity of tritium atoms in excess in the electrolytic solution in each cell was obtained by subtracting the averaged data $(q^{1}_{exp} - q^{1}_{th}) > 6.25 \times 10^{-2}$. The following equation was then used to calculate the integral curve of the excess of tritium atoms:

$$^3H\,|_0^t = 9.17 \times 10^6 \alpha_E x^0 V^0 \left\{ \int_0^t \left[\left(q^{\#}_{exp} - q^{\#}_{th} \right) - \overline{\left(q^{1}_{exp} - q^{1}_{th} \right)} \right] dt \right\} \quad (16)$$

by considering first that the combination of α_E and q allows us to write $x^{\#} = \alpha_E x^0 q^{\#}$ (see also Appendices A and B). As can clearly be seen in the bottom plot in Fig. 7, according to this procedure excess tritium is present only in the cells 2 and 8.

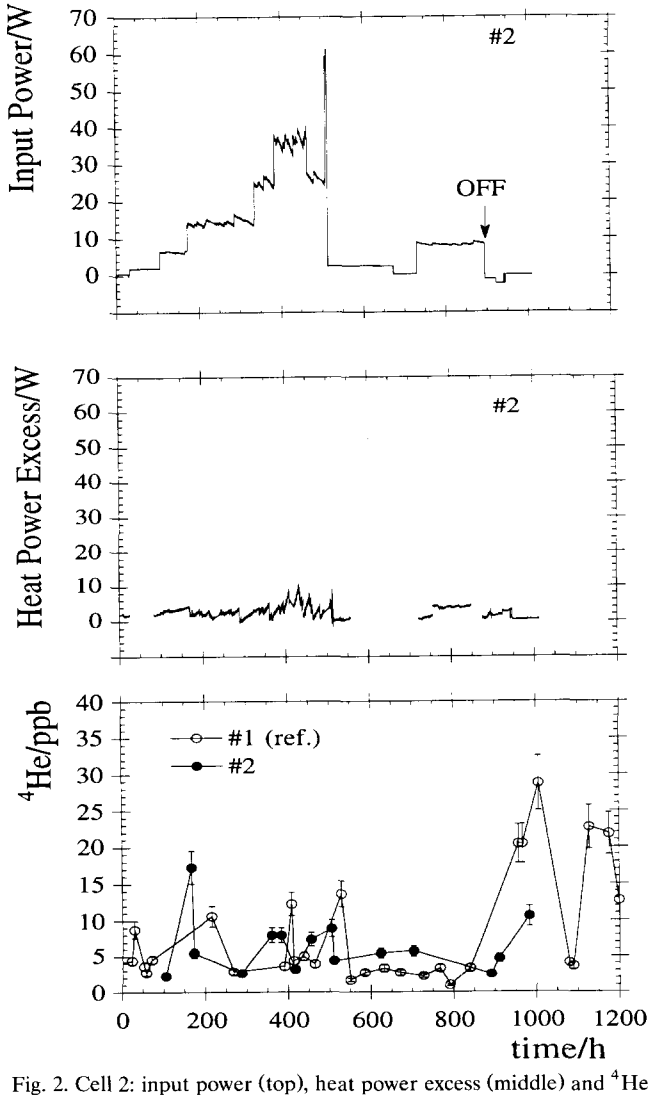

Fig. 2. Cell 2: input power (top), heat power excess (middle) and ^{4}He concentration in the gas stream of cell 2 and reference cell 1 (bottom).

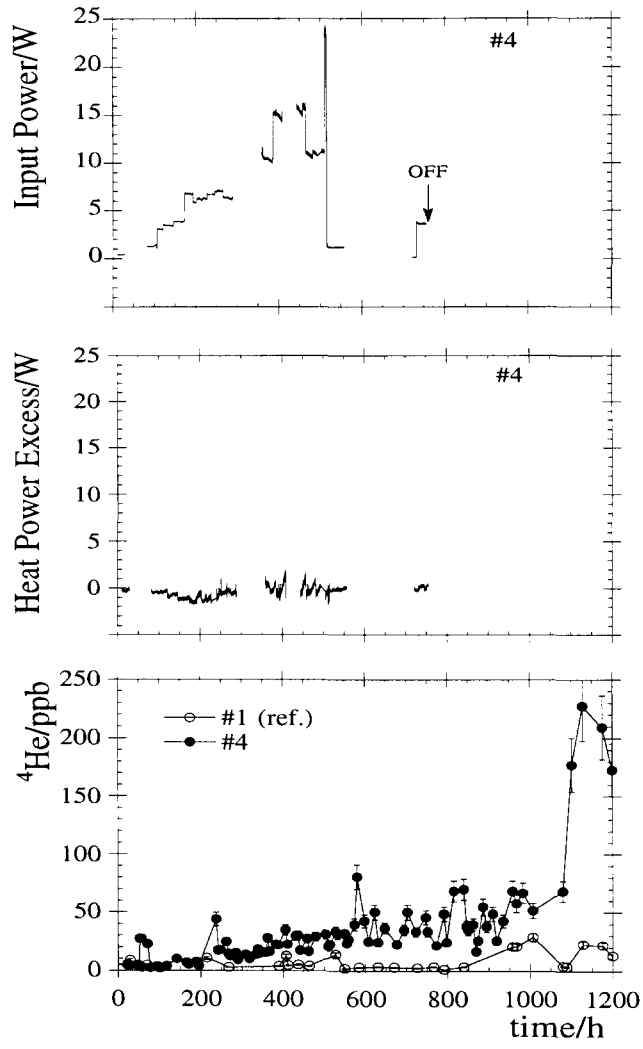

Fig. 3. Cell 4: input power (top), heat power excess (middle) and ^{4}He concentration in the gas stream of cell 4 and reference cell 1 (bottom).

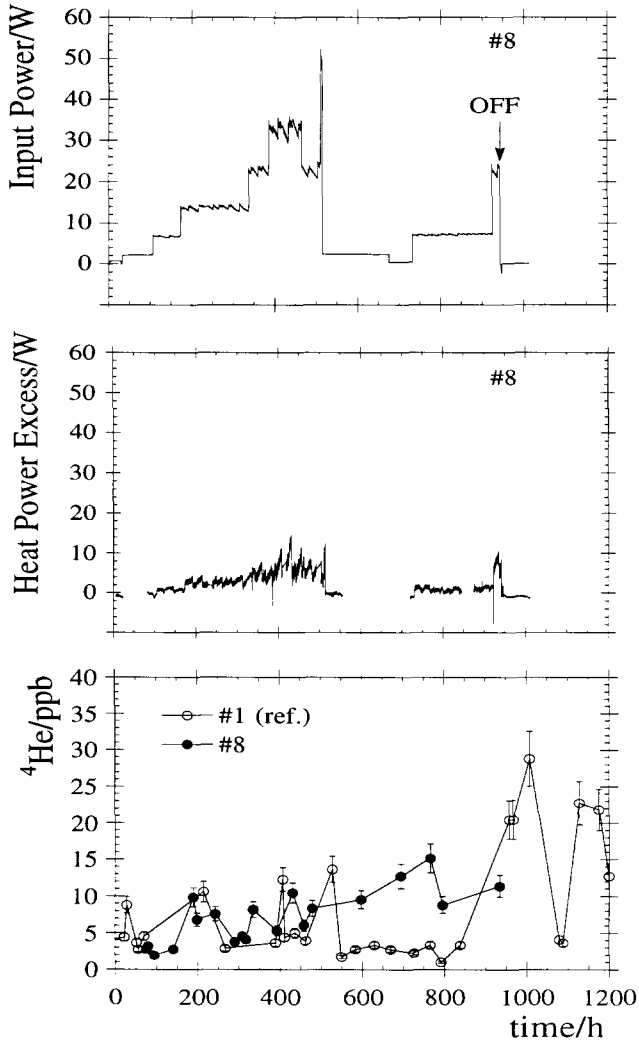

Fig. 4. Cell 8: input power (top), Heat power excess (middle) and ^{4}He concentration in the gas stream of cell 8 and reference cell 1 (bottom).

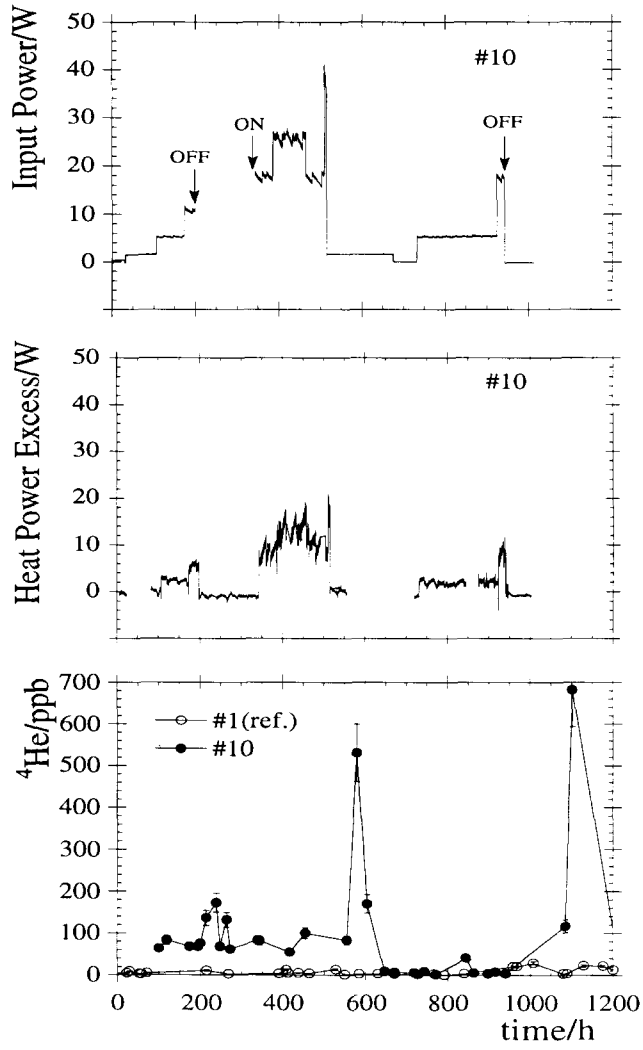

Fig. 5. Cell 10: input power (top), heat power excess (middle) and ^{4}He concentration in the gas stream of cell 10 and reference cell 1 (bottom).

3.3. Neutron data

This experiment showed no statistically significant evidence of neutron emission from the cells. Fig. 8 (bottom) shows the number of neutrons detected at 10 min intervals by the tube groups 1, 3, 6, 11 and 12 before and during the experiment. The graphs of neutron counts vs. time of the other groups, which are not shown, have similar characteristics and trends. As can be seen in the figure, there is no statistical difference between the number of neutrons detected when the electrolysis was in progress and the background. Ap-

Table 3
Summary of the calorimetric results

Cell no.	Cathode diameter/mm	Treatment	Current density [a]/mA cm^{-2}	Excess power [b]/W	Volume excess power/W cm^{-3}	Surface excess power/W cm^{-2}	Γ
2	2	No	1280	10.0 ± 1.0	111	6.4	0.26
4	6	Yes	460	2.0 ± 0.2	3	0.46	0.13
8	3	Yes	947	15.0 ± 1.5	79	7.1	0.43
10	3	No	905	19.0 ± 1.9	100	8.6	0.70

[a] Current density at the maximum excess power.
[b] Maximum excess power.

parent exceptions are the two large counts in group 12, which occurred at c. 900 h and c. 1200 h. However, simple considerations of the stabilization of the experimental apparatus together with an oscilloscope check of the pulses coming from the groups of tubes showed that the two large enhancements of the neutron counting rate of group 12 (as well other enhancements detected in other groups not shown in Fig. 8 but having the same characteristics) were not generated by neutrons but could be explained as follows. As shown in Fig. 8 (upper), the presence of two rings of groups of tubes surrounding the toroid embedding the cells ensures that a neutron bunch emitted from any cell (and also from the region outside the detector) must hit at least one group in each ring. Thus enhancements of the neutron counts of group 12, if generated by real neutrons, must be accompanied by simultaneous enhancements of at least one of the outer ring groups. In particular, groups 11 must also register an enhanced signal. The analogue signal coming from a group hit by a neutron, as checked by the oscilloscope, normally has an unusual negative shape (see Fig. 6 of ref. [24]). Thus the two enhancements of the neutron count detected by group 12 were generated by anomalous pulses, in

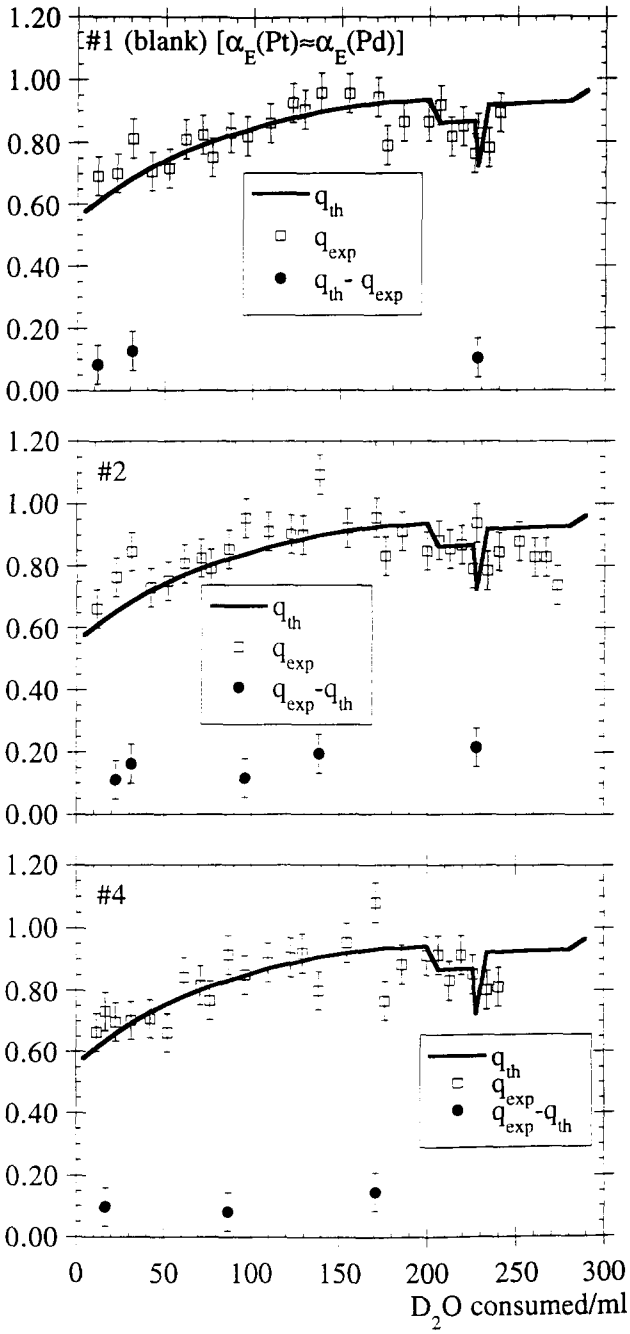

Fig. 6. Tritium in recombined gases: values of q_{th}, q_{exp} and ($q_{th} - q_{exp}$) for cells 1, 2 and 4.

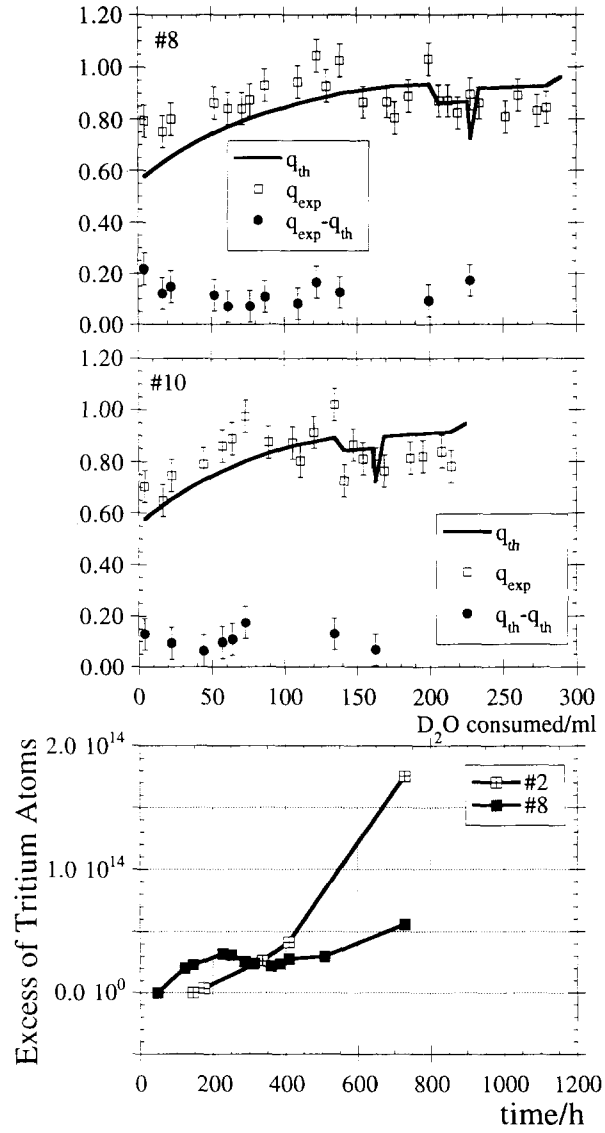

Fig. 7. Tritium in recombined gases: values of q_{th}, q_{exp} and ($q_{th} - q_{exp}$) for cells 8 and 10. The bottom plot shows the excess of tritium atoms for cells 2 and 8.

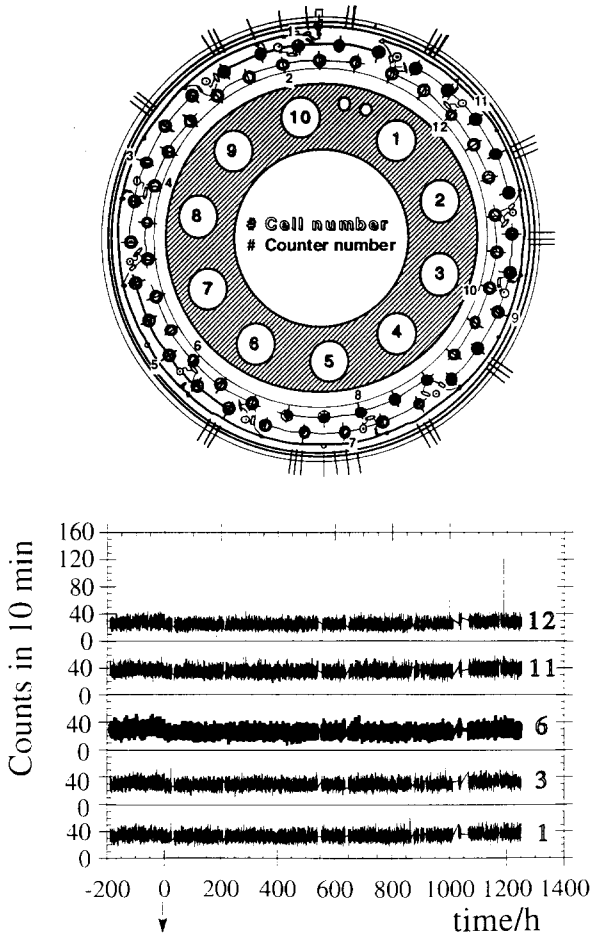

Fig. 8. Upper figure: top view of the 60 ^{3}He tubes, neutron counters and cell positioning in the torus. Bottom figure: counts every 10 min of five counting groups out of 12 before and after the start of the experiment.

which a sudden very large negative drop of the signal was followed by oscillations around zero.

4. Discussion

Owing to the absence of a significant neutron emission and the small excess of ^{3}H atoms with respect to the excess power measured, in the following we consider the nuclear reaction

$$d + d = {}^4He + 23.8\ MeV(lattice) \quad (17)$$

as the origin of the observed power excess. Therefore the most important comparison to be made is between the power excess and the ^{4}He found, assuming that reaction (17) is the source of both these quantities.

In order to compare the excess power data reported in Figs. 2–5 with the ^{4}He found, it is necessary to correlate the ^{4}He recovered with the time interval of its release. Because of the unknown and probably complex fluid dynamics of ^{4}He in the sampling cylinder we applied a straightforward assumption. The minimum sampling time mst, defined as the time required to fill a sampling cylinder of volume V_s at a gas flow rate J_G at the sampling stage (after the catalytic recombination), was defined as

$$mst = \frac{V_s}{J_G} = \frac{PV_s}{\left[(P/RT_r)f_{N_2} + (3/4F)(1-\eta)I\right]RT_r} \quad (18)$$

The quantity calculated corresponds to the time which an ideal piston would require to move at constant velocity from the bottom to the top of the sampling cylinder. This is equivalent to saying that the entering gas pushes out the pure N_2 initially present in the cylinder. According to this hypothesis, the composition of the gas trapped in the cylinder at sampling is representative of the gas composition during the last mst seconds before the sampling, independently of the flushing time. From Eq. (18) it appears that, under our experimental conditions, the mst value is confined within a short range of variability and, in any case, is at least 12 times less than the typical sampling time (ca. 3 h) that we actually used [28]. As expected from this equation, for $\eta \to 1$, mst is independent of the value of the electrolysis current.

Therefore if the excess heat power is known, by considering the mass flux balance in the cell it is possible to calculate the expected ^{4}He concentration $x_{^4He}$, produced through reaction (17) in the sampled gas stream:

$$x_{^4He} = \frac{(q_r/N_A)\int_0^t P_{exc}\,dt}{(P/RT_r)f_{N_2}t + (3/4F)(1-\eta)\int_0^t I\,dt + (q_r/N_A)\int_0^t P_{exc}\,dt} \approx \frac{(q_r/N_A)P_{exc}}{(P/RT_r)f_{N_2} + (3/4F)(1-\eta)I} \quad (19)$$

The approximation implies that P_{exc} is constant with time over the integration interval and that the contribution of the ^{4}He flux is negligible with respect to the sum of the other fluxes. From Eq. (19) it can be seen that the ^{4}He concentration measurable in the gas stream depends on various experimental parameters which must be kept under control. For $\eta \to 1$, the quantity $\partial x_{^4He}/\partial P_{exc}$, derived from Eq. (19), becomes independent of I. To convert the experimental concentration values (in ppb) of ^{4}He into excess power, the following equation was used:

$$\overline{P_{exc}} = 10^{-9} e n_{tot} q_r \frac{x_{^4He}}{mst} = 46.9788 \frac{x_{^4He}}{mst} \quad (20)$$

where $n_{tot} = N_A PV_s/RT_r$ is the total number of molecules in the sampling cylinder, $\overline{P_{exc}}$ calculated by Eq. (20) must be averaged over mst. Therefore the error in $\overline{P_{exc}}$ takes the same value as that in $x_{^4He}$ (13%).

The bottom plots in Figs. 9 and 10 show the heat power excess, as obtained by calorimetry, for cells 4 and 10 respectively (see middle plots of Figs. 3 and 5), and the top plots show the heat power excess calculated from ^{4}He data using Eq. (20) (see bottom plots of Figs. 3 and 5). It is important to observe that in each plot in Figs. 9 and 10 the two heat power excess quantities, which were obtained in a completely independent way, are commensurate (note that the limits of the ordinate scales are the same in each plot). It is evident from the time structure shown in Figs. 9 and 10 that two different processes are at work, and in both the cases the ^{4}He concentrations are clearly higher than the respective ^{4}He backgrounds before the start of the experiment (not for cell 10 because we have no background) apart from the background found in the blank cell 1. If we limit consideration to the time interval where electrolysis is still taking place (see Fig. 1), we observe for cell 4 a progressive increase of the heat power excess from ^{4}He (HPEH) compared with a quite constant and low heat power excess from calorimetry (HPEC). The trend is clear even when the errors on both quantities are taken into account, although at any time (HPEH $\pm$ ΔHPEH) $\approx$ (HPEC $\pm$ ΔHPEC) holds. In cell 10, the result (HPEH $\pm$ ΔHPEH) > (HPEC $\pm$ ΔHPEC) is found only when the

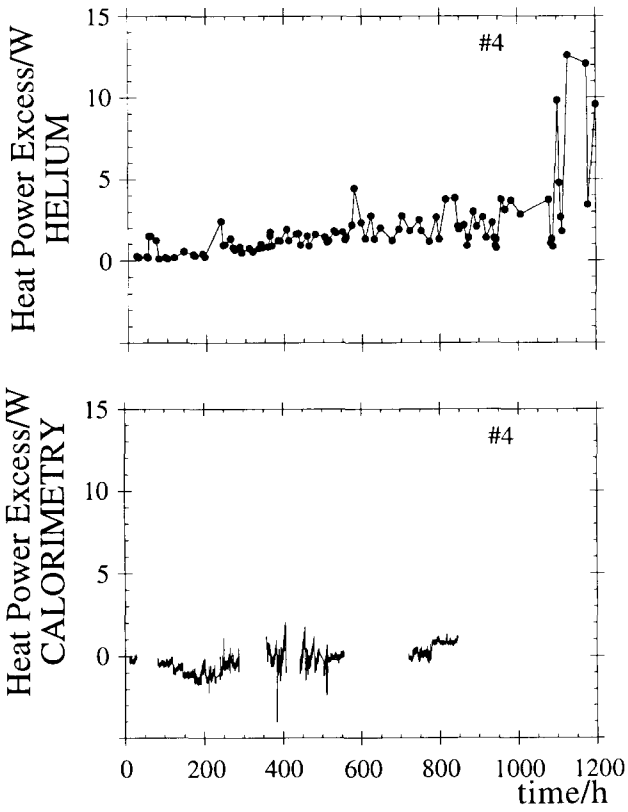

Fig. 9. Cell 4: heat power excess calculated from ^{4}He data (reaction (17) and Eq. (20)) (upper plot) and as measured by calorimetry (bottom plot).

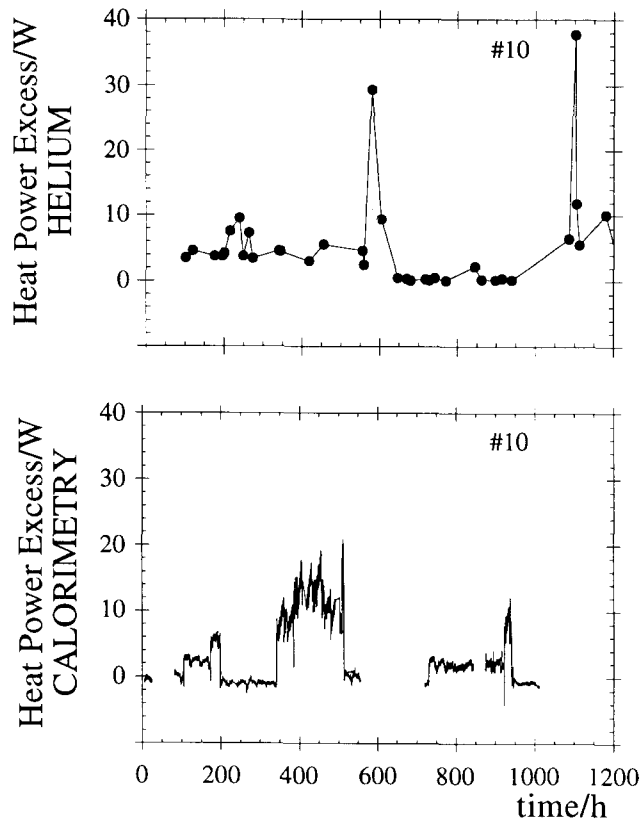

Fig. 10. Cell 10: heat power excess calculated from ^{4}He data (reaction (17) and Eq. (20)) (upper plot) and as measured by calorimetry (bottom plot).

electrolysis current is very small or switched off. In all other cases, HPEC prevails. What is impressive is that ^{4}He recovery is observed systematically after generation of excess heat. The evaluation of ΔHPEC has been discussed in Section 2, and while ΔHPEH can be obtained directly from Eq. (20) as it is proportional to the error in the ^{4}He determination [28]. The application of Eq. (20) to the ^{4}He data from cells 2 and 8 (Figs. 2 and 4 respectively) gives HPEH values below 0.6 ± 0.1 W after subtracting the ^{4}He background present before electrolysis. This value is better than (but comparable with) the calorimetric detection limit shown in Table 2. According to Eq. (19) and the maximum HPEC found, the corresponding maximum values of ^{4}He concentration expected for cells 2 and 8 should be 195 ppb and 202 ppb respectively. This is not in agreement with the experimental findings. Similar reasoning gives better agreement for cell 10 and, to some extent, for cell 4. Therefore we are apparently left with the dilemma of one cell which shows a ^{4}He concentration in the gas phase of the correct order of magnitude (with respect to the heat excess) but two others (cells 2 and 8) which do not. However, before drawing any particular conclusion, two central questions must be answered.

Is there a time relation between the heat generation and ^{4}He release from the surface?

If there is, is the delay a function of how deep the source is with respect to the electrode surface?

To our knowledge, the experimental evidence required to answer these questions satisfactorily is not yet available. It has been reported [33,34] that ^{3}He or ^{4}He are highly insoluble in metals and that they nucleate everywhere that point or linear defects exist. The transformation from a cluster of a few atoms to a microbubble depends on the extent of the defect and/or the ability of the defects to migrate. In any case, the probability that a bubble will reach the surface is very low, and increases as the distance between the nucleation site and the surface decreases. If this distance becomes greater than 10 nm, the time required for ^{4}He to reach the surface could be as long as 14 years [35]. So far we have dealt with a scheme applicable to all the metals and alloys, but matters could change radically in the case of a Pd specimen subject to a process where defects are generated continuously and propagate randomly in the metallic matrix owing to D charging. In this case, ^{4}He could reach the surface via the defects produced by D loading (sometimes so extended that they could collapse, generating fractures). In this case we could not expect any correlation between the times of heat generation and ^{4}He release, except if the site of the nuclear reaction is on the surface itself or a few monolayers below. Therefore it is unlikely that the recovery of ^{4}He in the gas phase of different electrodes (and therefore different microstructures) will occur at any definite and predictable rate. Hence, under this hypothesis, our results for heat excess and ^{4}He retain their significance. In view of the above considerations, the condition HPEH $\leq$ HPEC should be expected.

Experimental evidence consistent with the reasoning above in which the energy related to ^{4}He production was about an order of magnitude lower than the energy excess found by calorimetry, has been reported [3].

The integration of the HPEH and HPEC data of cell 10 given in Fig. 10 is shown in Fig. 11. Throughout the experiment the heat excess from ^{4}He is found to be commensurate with the heat excess measured by calorimetry, although the former is observed over longer time intervals than the latter (200–500 h compared with 600–1050 h).

According to the reasoning above this is not allowed. However, as already mentioned, the detection of ^{20}Ne [28] suggests that at least partial air contamination may have occurred [3], and this extra source of ^{4}He could account for the discrepancy. With regard to the

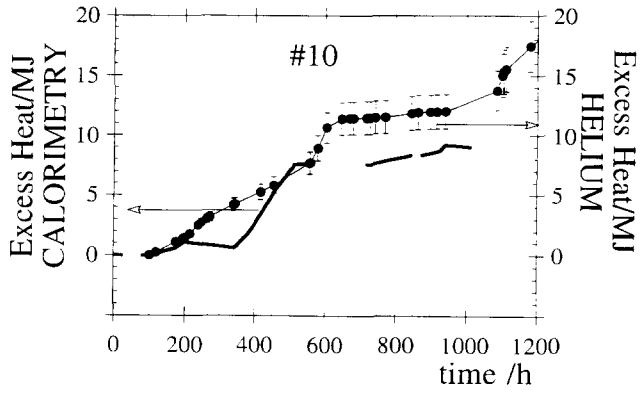

Fig. 11. Cell 10: comparison of heat excess obtained by integration over time of heat power excess as measured by calorimetry (Fig. 5, middle plot) with the heat excess obtained by integration of Eq. (20) over time.

error bar on the solid curve of Fig. 11, the same considerations given before for the other curves showing calorimetric data still hold.

It should be noted that in the plots of Figs. 6 and 7 for the tritium data there are a small number of experimental points $q^{\#}_{exp}$ which not only exceed the expected value $q^{\#}_{th}$ over the experimental error but are greater than or equal to unity. It is easy to demonstrate from Eq. 13 that, in absence of tritium generation, the condition $q_{lim} \geq 1$ would produce the result $\alpha_E/\alpha_V \leq 1$ which is clearly impossible because $\alpha_E > 1$ and $\alpha_V \approx 1$. This constitutes a strong and rigorous support favouring the generation of tritium, even if this appears to occur sporadically at low level. However, it is important to recall that the tritium measurement is not an on-line measurement and since it is performed on the recombined D_2O, the minimum time interval between two samplings is the time necessary to produce at least 1 ml of D_2O which is a suitable volume for determining the tritium. This time is given by $2F/\bar{v}I\eta$. Consideration of the current plots (Fig. 1) shows that the time required varies from ca. 1 h (at $I = 2.5$ A) to ca. 33 h (at $I = 0.1$ A). For practical reasons it was not possible for us to perform the tritium test for every 1 ml of D_2O produced, particularly at the highest current values, and so the sampling (of 1 ml) was frequently made on a higher volume of D_2O. In the case of stepwise release of tritium in the cell, as may be expected, this implies that this time structure is lost because of the dilution effect which flattens the concentration profile. A further important point, which is often insufficiently stressed in discussing tritium measurements, is the distribution of any tritium generated. In our opinion, which is supported in the literature [36,37], tritium should be sought in the cathode and/or the gas phase. In fact, if tritium is produced in the bulk of the cathode, it can be trapped and/or eventually released

[3] Without invoking the concurrent release of both ^{4}He and ^{20}Ne.

as DT (g). If the DT molecules are generated at the surface, they enter the gas phase directly. According to the mechanism generally adopted [38] for the electrolytic reduction of H(D) on a cathode (Me), the H_2 (D_2) formation step can follow two different processes:

$$D_{ads}(Me) + D_{ads}(Me) = D_2(g) \quad (21a)$$

and/or

$$D_{ads}(Me) + D_2O + e^-(Me) = D_2(g) + OD^- \quad (21b)$$

If tritium atoms (T) are produced at the Me surface, reactions (21) become

$$D_{ads}(Me) + T_{ads}(Me) = DT(g) \quad (22a)$$

and/or

$$T_{ads}(Me) + D_2O + e(Me) = D_2(g) + OT^- \quad (22b)$$

If step (22b) is followed, it is possible to keep tritium in the solution as has been found and reported previously [20,24,25]. None of the other processes allows tritium to remain in the solution in significant amounts since the dissolution of DT in D_2O and the catalysed reaction of T at the cathode with dissolved oxygen in solution to give DTO, are negligible processes. Therefore a complete tritium balance would require its measurement in both the Pd cathode and the solution. Furthermore, if tritium is measured in the gas phase via the external catalytic recombination, as was done here, two factors may combine to give an underestimated result: (i) the isotopic effect on the catalytic recombination which increases the rate of the D_2O formation with respect to DTO; (ii) the stoichiometric ratio $D_2/O_2 = 2$, fixed by the electrolysis and exactly suitable for the recombination, is no longer strictly satisfied in the recombinator when tritium is generated because $(D_2 + DT)/O_2 > 2$.

From the bottom plot of Fig. 7, it appears that a net production of tritium atoms occurs only in the cells 2 and 8. In these cells ^{4}He was found to be very low and not comparable with the excess heat.

If the tritium channel of the d,d reaction of plasma fusion is invoked, we can calculate that the energy released throughout the experiment in the case of cell 2, for instance, is 115 J, whereas a rough estimate of the integrated heat excess measured by calorimetry in the same cell (see Fig. 2) is more than four orders of magnitude greater. By the same reasoning, we should expect an excess of neutrons with respect to the background which is equal to the number of tritium atoms. This would imply a maximum averaged rate of ca. 7×10^7 ns^{-1}. This rate, in addition to being very dangerous, would be easily detectable but, as shown in Fig. 8, no excess of neutrons above the background was measured.

5. Conclusions

Our calorimetric results show an excess power which is quite in line with the other positive results reported up to now. In particular, if we consider the power excess per unit electrode surface area as a function of the current density, fair agreement is found with the general behaviour first pointed out by Storms [27] by considering that many calorimetric measurements on the Pd + D_2O electrolysis were carried out at room temperature in various laboratories where different calorimetric devices and procedures were used. With regard to the nuclear products, in the present experiment a lack of neutrons and a low tritium excess on two out of four cells has been observed, in contrast with what is expected on the basis of d,d reactions. Our results confirm the previous findings which exhibited such a large unbalance. As for the ^{4}He measurements in the escaping gases, the detection of ^{20}Ne [28] prevents a definite conclusion to be drawn from comparisons with the calorimetric data. However, the notable commensurate amounts of ^{4}He and heat excess found in the case of cell 10 cannot be ignored. The time pattern of the amount of ^{4}He recovered, which, although shifted in time, matches the power excess time pattern observed, is also quite striking. The different quantities of ^{4}He recovered from different cells (e.g. cells 8 and 10), where power excesses of the same order of magnitude have been observed, are understandable if different kinetics of the ^{4}He release are invoked, and they highlight the usefulness of being able to perform a complete energy and mass balance analysis which also includes the ^{4}He content of the electrodes.

Acknowledgments

The financial support of the National Research Council (CNR), the National Institute of Nuclear Physics (INFN) and the Physics Laboratory of the Istituto Superiore di Sanità are gratefully acknowledged. We are grateful to Dr. M. Achilli and Professor E. Cardarelli for performing the ICPAES chemical analyses and to Dr. D. Ferro for the skilful SEM analysis of the cathodes.

Appendix A. Symbols

a_{D_2}	activity of D_2 in the gas phase
a_i	intercept of the calibration curve of the ith cell, W
b_i	slope of the calibration curve of the ith cell, W °C^{-1}
C_g	heat capacity of D_2O vapour, J mol^{-1} K^{-1}

C_l heat capacity of D_2O liquid, J mol^{-1} K^{-1}
C_r relative capacity of Pd sponge trap
C_S heat capacity of solution, J mol^{-1} K^{-1}
C_{trap} nominal capacity of Pd sponge trap for D_2, mol
$\bar{d}$ deuterium nuclei
d inner diameter of cell, mm
f_{D_2O} feed of D_2O to the cell, mol s^{-1}
f_G gas flow rate of the gas mixture, mol s^{-1}
f_{N_2} N_2 flow rate, scm^3 s^{-1}
f_{cond} correction for D_2O condensation in recombinator, cm^3 s^{-1}
h height of the solution level in the cell, mm
I electrolysis current, A
k_{Pyrex} thermal conductivity of Pyrex, W m^{-1} K^{-1}
k_{rad} Stefan–Boltzmann constant, W m^2 K^{-4}
l thickness of Pyrex wall of the cell, mm
M molar mass of D_2O, g mol^{-1}
M_{Pd} atomic mass of Pd, g mol^{-1}
m_s mass of solution, mol
mst minimum sampling time, s
n_{D_2O} number of moles of D_2O in V^0
n_{tot} total number of molecules in V_s
P atmospheric pressure, kPa
p vapour pressure of D_2O, Pa
p_{D_2} D_2(g) partial pressure, atm
$P_{exc,i}$ excess of heat power of the ith cell, W
P_{in} input power, W
P_{out} output power, W
r correlation factor in linear regression
T_r room temperature, °C
T_s solution temperature, °C
T_s^0 solution temperature at $P_{in} = 0$, °C
T_{tb} temperature of thermostated bath, °C
T_{tb}^0 temperature of thermostated bath at $P_{in} = 0$, °C
V_{in} input voltage of the cell, V
v_{cons} volume of D_2O consumed by electrolysis, cm^3
v_{rec} volume of D_2O recombined, cm^3
$\bar{v}$ molar volume of D_2O, cm^3 mol^{-1}
V_s volume of the sampling bottle, cm^3
V_{th} thermoneutral potential, V
V^0 volume of solution in the cell, cm^3
w_{Pd} weight of Pd sponge in the trap, g
x atomic fraction of DTO in D_2O
x_f atomic fraction of DTO in D_2O feed
$x_{^4He}$ atomic fraction of ^4He in the gas mixture
x_g atomic fraction of tritium in the gas mixture
x^0 starting atomic fraction of DTO in the electrolyte
y D/Pd atomic ratio

α_E x_g/x, electrolytic separation factor
α_V x_g/x, isotopic separation factor in the vaporization
ΔH^0 standard enthalpy change of formation of D_2O, kJ mol^{-1}
ΔH_{abs} enthalpy change of reaction (8), kJ mol^{-1}
ΔS_{abs}^0 standard entropy change of reaction (8), J mol^{-1} K^{-1}
ΔT_i $\Delta T_i = (T_s - T_s^0)_i - (T_{tb} - T_{tb}^0)_i$, °C
Γ ratio of excess power to input power
η recombination yield
Λ heat of evaporation of D_2O, J mol^{-1}
ρ_l density of D_2O, kg m^{-3}
τ time constant, s

Appendix B. Constants

C_g heat capacity of D_2O vapour 44.500 J mol^{-1} K^{-1}
C_l heat capacity of D_2O liquid 84.349 J mol^{-1} K^{-1}
C_{trap} nominal capacity of Pd sponge trap c. 0.47 D_2 mol
d inner diameter of cell 22.0 mm
e elementary charge 1.60219×10^{-19} C
F Faraday constant 96484.6 C mol^{-1}
f_{N_2} N_2 flow-rate 0.54 scm^3 s^{-1}
h height of the solution level in the cell c. 180 mm
k_{Pyrex} thermal conductivity of Pyrex 0.878 W m^{-1} K^{-1}
k_{rad} Stefan–Boltzmann constant 5.6703×10^{-8} W m^2 K^{-4}
l thickness of Pyrex wall of the cell 2 mm
M molar mass of D_2O 20.02748 g mol^{-1}
M_{Pd} atomic mass of Pd 106.42 g mol^{-1}
N_A Avogadro's number 6.02205×10^{23} mol^{-1}
P Atmospheric pressure 101.3 kPa (nominal)
p vapour pressure of D_2O 7.83×10^2 exp(5.143×10^{-2} T_S) Pa
p_{DTO} vapour pressure of DTO 7.66×10^2 exp(-5.165×10^{-2} T_S) Pa
q_s atomic fraction of ^4He in the gas mixture 23.8 MeV
R ideal gas constant 8.31441 J mol^{-1} K^{-1}
T_r room temperature 20 ± 1°C
T_{tb} temperature of thermostated bath 21.0 ± 0.1°C
$\bar{v}$ molar volume of D_2O 18.116 cm^3 mol^{-1}
V_s volume of the sampling bottle 500 cm^3
V_{th} thermoneutral potential 1.53668 V
V^0 volume of solution in the cell c. 53 cm^3
$x^0 = x_f$ starting atomic fraction of DTO in the electrolyte [4] 80 dpm ml^{-1}

[4] 1 dpm = 1 disintegration per minute = 9.17×10^6 atom T min^{-1} = 4.50×10^{-7} μCi.

y	D/Pd atomic ratio (at 298 K, $p_{D_2} = P$) 0.67
α_E	electrolytic separation factor 1.8
α_V	isotopic separation factor in vaporization c. 1
ΔH^0	standard enthalpy of formation of D_2O 296.53 kJ mol^{-1}
ΔH_{abs}	enthalpy change of reaction (8) $\Delta H_{abs}(y) = 95.5 - 89.96y$ kJ mol^{-1}
ΔS^0_{abs}	standard entropy change of reaction (8) 106.3 J mol^{-1} K^{-1}
Λ	heat of evaporaiton of D_2O 41.673 kJ mol^{-1}
ρ_l	density of D_2O 1.1055 g cm^{-3}

References

[1] M. Fleischmann and S. Pons, Phys. Lett. A, 176 (1993) 118.
[2] D. Albagli et al., J. Fusion Energy, 9 (1990) 133.
[3] B.F. Bush, J.J. Lagowski, M.H. Miles and G.S. Ostrom, J. Electroanal. Chem., 304 (1991) 271.
[4] N. Lewis et al., Nature (London), 340 (1989) 525.
[5] M.H. Miles, R.A. Hollins, B.F. Bush, J.J. Lagowski and R.E. Miles, J. Electroanal. Chem., 346 (1993) 99.
[6] E. Yamaguchi and T. Nishioka in H. Ikegami (Ed.), ICCF3, Proc. 3rd Int. Conf. on Cold Fusion, Nagoya, 21–25 October 1992, Frontiers of Science Series 4, Universal Academy Press, Tokyo, 1993, p. 179.
[7] J. O'M. Bockris, C.C. Chien, D. Hodko and Z. Minovski in H. Ikegami (Ed.), ICCF3, Proc. 3rd Int. Conf. on Cold Fusion, Nagoya, 21–25 October 1992, Frontiers of Science Series 4, Universal Academy Press, Tokyo, 1993, p. 231.
[8] B.Y. Liaw and P.L. Tau, J. Electroanal. Chem., 319 (1991) 161.
[9] P.L. Hagelstein, J. Fusion Energy, 9 (1991) 451. P.L. Hagelstein, ICCF4, Proc. 4th Int. Conf. on Cold Fusion, Lahaina, HI, 6–9 December 1993, EPRI, Palo Alto, CA, in press.
[10] G. Preparata in T. Bressani, B. Minetti and A. Zenoni (Eds.), Common Problems and Ideas of Modern Physics, World Scientific, 1992. G. Preparata in T. Bressani, E. Del Guidice and G. Preparata (Eds.), ACCF2, Proc. 2nd Annu. Conf. on Cold Fusion, Como, 29 June–4 July 1991, Conf. Proc. Ital. Phys. Soc., 33 (1991) 453.
[11] J. Schwinger, Z. Phys. D, 15 (1990) 21; Z. Naturforsch. A, 45 (1990) 756. J. Schwinger, ICCF4, Proc. 4th Int. Conf. on Cold Fusion, Lahaina, HI, 6–9 December 1993, EPRI, Palo Alto, CA, in press.
[12] H. Rambaut and J.P. Vigier, Phys. Lett. A, 142 (1989) 447; 148 (1990) 229; 163 (1992) 335.
[13] ACCF1, Proc. 1st Annu. Conf. on Cold Fusion, Salt Lake City, UT, 28–31 March 1990.
[14] T. Bressani, E. Del Guidice and G. Preparata (Eds.), ACCF2, Proc. 2nd Annu. Conf. on Cold Fusion, Como, 29 June–4 July 1991, Conf. Proc. Ital. Phys. Soc., 33 (1991).
[15] H. Ikegami (Ed.), JCCF3, Proc. 3rd Int. Conf. on Cold Fusion, Nagoya, 21–25 October 1992, Frontiers of Science Series 4, Universal Academy Press, Tokyo, 1993.
[16] ICCF4, Proc. 4th Int. Conf. on Cold Fusion, Lahaina, HI, 6–9 December 1993, EPRI, Palo Alto, CA, in press.
[17] Workshop on Cold Fusion Phenomena, Santa Fé, NM, 22–25 May 1989, J. Fusion Energy, 9 (1990).
[18] S. Jones, F. Scaramuzzi and D. Worledge (Eds.), Anomalous Nuclear Effects in Deuterium/Solid Systems, AIP Conf. Proc., 228 (1991).
[19] D. Gozzi, P.L. Cignini, L. Petrucci, M. Tomellini, G. De Maria, S. Frullani, F. Garibaldi, F. Ghio and M. Jodice in R.A. Ricci, E. Sindoni and F. De Marco (Eds.), Understanding Cold Fusion Phenomena, Conf. Proc. Ital. Phys. Soc., 24 (1989).
[20] D. Gozzi, P.L. Cignini, L. Petrucci, M. Tomellini, G. De Maria, S. Frullani, F. Garibaldi, F. Ghio and M. Jodice, Nuovo Cim. 103A (1990) 143.
[21] M. Tomellini and D. Gozzi, J. Mater. Sci. Lett., 9 (1990) 836.
[22] D. Gozzi, P.L. Cignini, L. Petrucci, M. Tomellini, G. De Maria, S. Frullani, F. Garibaldi, F. Ghio, M. Jodice and E. Tabet, J. Fusion Energy, 9 (1990) 241.
[23] D. Gozzi, P.L. Cignini, L. Petrucci, M. Tomellini, S. Frullani, F. Garibaldi, F. Ghio, M. Jodice and G.M. Urciuoli in S. Jones, F. Scaramuzzi and D. Worledge (Eds.), Anomalous Nuclear Effects in Deuterium/Solid Systems, AIP Conf. Proc., 228 (1991) 481.
[24] D. Gozzi, P.L. Cignini, M. Tomellini, S. Frullani, F. Garibaldi, F. Ghio, M. Jodice and G.M. Urciuoli, Fusion Technol., 21 (1992) 60.
[25] D. Gozzi, P.L. Cignini, M. Tomellini, S. Frullani, F. Garibaldi, F. Ghio, M. Jodice and G.M. Urciuoli in T. Bressani, G. Del Guidance and G. Preparata (Eds.), ACCFZ, Proc. 2nd Annu. Conf. on Cold Fusion, Como, 29 June–4 July 1991, Conf. Proc. Ital. Phys. Soc., 33 (1991) 21.
[26] D. Gozzi, P.L. Cignini, R. Caputo, M. Tomellini, G. Balducci, G. Gigli, E. Asbani, S. Frullani, F. Garibaldi, M. Jodice and G.M. Urciuoli in H. Ikegami (Ed.), ICCF3, Proc. 3rd Int. Conf. on Cold Fusion, Nagoya, 21–25 October 1992, Frontiers of Science Series 4, Universal Academy Press, Tokyo, 1993, p. 155.
[27] E. Storms, Fusion Technol., 20 (1991) 433.
[28] D. Gozzi, R. Caputo, P.L. Cignini, M. Tomellini, G. Gigli, G. Balducci, E. Asbani, S. Frullani, F. Garibaldi, M. Jodice and G.M. Urciuoli, J. Electroanal. Chem., 380 (1994) 109.
[29] J. Balej and J. Divisek, J. Electroanal. Chem., 278 (1989) 85.
[30] R.C. Weast (Ed.), Handbook of Physics and Chemistry (60th ed.) CRC Press, Boca Raton, FL, 1980.
[31] G. Alefeld and J. Völkl (Eds.), Hydrogen in Metals, Vol. II, Springer-Verlag, Heidelberg, 1978, p. 95.
[32] D. Gozzi et al., in preparation.
[33] E. Ruedl et al., Proc. Conf. on Research, Development and Technology of Fusion Reactor Materials, ENEA, Frascati, December 1990. F. Carsughi et al., Proc. Conf. on Research, Development and Technology of Fusion Reactor Materials, ENEA, Frascati, 4–6 December 1990. P. Gondi, Proc. Conf. on Research, Development and Technology of Fusion Reactor Materials, ENEA, Frascati, 4–6 December 1990.
[34] G.J. Thomas and J.M. Mintz, J. Nucl. Mater., 116 (1983) 336.
[35] M.W. Lee, ICCF4, Proc. 4th Int. Conf. on Cold Fusion, Lahaina, HI, 6–9 December 1993, EPRI, Palo Alto, CA, in press.
[36] F.G. Will, K. Cedzynska and D.C. Linten, ICCF4, Proc. 4th Int. Conf. on Cold Fusion, Lahaina, HI, 6–9 December 1993, EPRI, Palo Alto, CA, in press.
[37] K. Cedzynska, S.C. Barrowes, H.E. Borgeson, L.C. Knight and F.G. Will in S. Jones, F. Scaramuzzi and D. Worledge (Eds.), Anomalous Nuclear Effects in Deuterium/Solid Systems, AIP Conf. Proc., 228 (1991) 463. K. Cedzynska, S.C. Barrowes, H.E. Bergeson, L.C. Knight and F.G. Will, Fusion Technol., 20 (1991) 108; 22 (1992) 156.
[38] J. O'M. Bockris and A.K.N. Reddy, Modern Electrochemistry, Vol. 2, Plenum, New York, 1974, Ch. 10.